Mitigating Damage to Hybrid Perovskites Using Pulsed-Beam TEM

Elisah J. VandenBussche, Catherine P. Clark, Russell J. Holmes, and David J. Flannigan*

Department of Chemical Engineering and Materials Science, University of Minnesota, 421 Washington Avenue SE, Minneapolis, MN 55455, USA

Using a 300-femtosecond pulsed laser to generate a pulsed electron beam in a modified TEM, we discover a clear and repeatable reduction in damage to $MAPbI_3$ as compared to conventional (random) beams delivered at the same dose rates and total doses. For a dose rate of 0.001 $e \cdot Å^{-2} \cdot s^{-1}$, we find a 17% reduction in damage for a pulsed beam with 50.4 ± 1.0 electrons per pulse, a beam size of 245 ± 3 μm^2, and a repetition rate of 500 kHz (2 μs between pulses). The overall damage increases with increasing number of electrons in each pulse (tested 50, 100, 200, and 400), while decreasing the duration elapsed between each pulse from 4 μs to 2 μs also produces a lesser but still significant increase. For a dose rate of 0.01 $e \cdot Å^{-2} \cdot s^{-1}$, a beam consisting of 400 electrons per pulse with 4 μs between each pulse causes more damage than a conventional beam, illustrating a threshold effect. Mechanistic origins centered on thermal and charging effects, as well as electron-phonon coupling and lattice-thermalization times in $MAPbI_3$, are discussed.

Comprehensive understanding of high power-conversion efficiencies of hybrid organic-inorganic perovskites (HOIPs) photovoltaic cells requires elucidation of atomic and nanoscale properties and behaviors of these materials.[1-3] Structural, chemical, electronic, and dynamic properties at this scale are accessible with transmission electron microscopy (TEM), but the stability of HOIPs is such that electron-beam damage can be significant.[4-7] Indeed, sensitivity of HOIPs to even low dose rates may limit what can be learned about fundamental structure/function relationships.[8-10] This damage is thought to occur through a combination of charging, ionic excitation, and heating leading to ion migration and separation of the organic and inorganic constituents.[10,11] As such, a number of methods, such as cryo-electron microscopy and low-dose imaging and diffraction, have been used to reduce deleterious beam effects.[12-14]

Femtosecond (fs) laser-driven and picosecond chopped-beam sources in modified TEMs offer additional means for mitigating damage.[15-19] These methods employ temporally-modulated beams, where electrons are delivered to the specimen in discrete pulses with well-defined durations between each, rather than in the random fashion of conventional sources (*e.g.*, thermionic). Indeed, time-dependent aspects of charging and thermal energy, as well as the dynamic self-healing properties of HOIPs, suggest there may be advantages to delivering dose in the form of well-timed pulses.[5,20-22] Here we explore fs laser-driven pulsed TEM for mitigating damage to HOIPs, specifically methylammonium lead iodide ($CH_3NH_3PbI_3$ or $MAPbI_3$). Our main goal was to determine – all else being equal – if a pulsed beam leads to a reduction in $MAPbI_3$ damage compared to a conventional beam. Accordingly, we focused on quantitatively comparing damage caused by pulsed beams to that of conventional thermionic beams *at the same dose rates and the same total doses*. We also studied the effects of the number of electrons per pulse (e/p) and the duration between pulse arrival at the specimen (f^{-1}, where f is the laser

repetition rate). We find a clear reduction in damage for pulsed beams compared to random (thermionic) beams, as well as an apparent exacerbation of damage with increasing instantaneous dose (*i.e.*, with more electrons per pulse) even with longer time elapsed between the arrival of each. We also observe a thresholding effect, where pulsed beams become more detrimental than random beams.

Beam-damage mechanisms in TEM are numerous and often synergistic, necessitating detailed design and systematic execution of experiments.[4,23] Conveniently, fs pulsed lasers in a stable lab environment afford high levels of control, enabling accurate and precise quantification of pulsed TEM beam damage.[17] An overview of the fs laser-driven approach used here, and the method for quantifying damage to MAPbI$_3$ specimens, is shown in Figure 1. Temporal regularity of the pulsed electron beam was accomplished using a 300-fs pulsed laser (PHAROS, Light Conversion), which confines electron emission to a train of 300-fs windows spaced in time by f^{-1}. The pulse train was generated *via* the photoelectric effect in a modified TEM (Tecnai Femto, Thermo Fisher) using ultraviolet laser pulses ($hv = 4.8$ eV) and a LaB$_6$ electron source ($\varphi = 2.4$ eV; Fig. 1a). Dose rate was controlled with both the laser-pulse fluence (which dictates e/p) and f (which dictates the number of pulses per second and the specimen relaxation time between each pulse, f^{-1}).
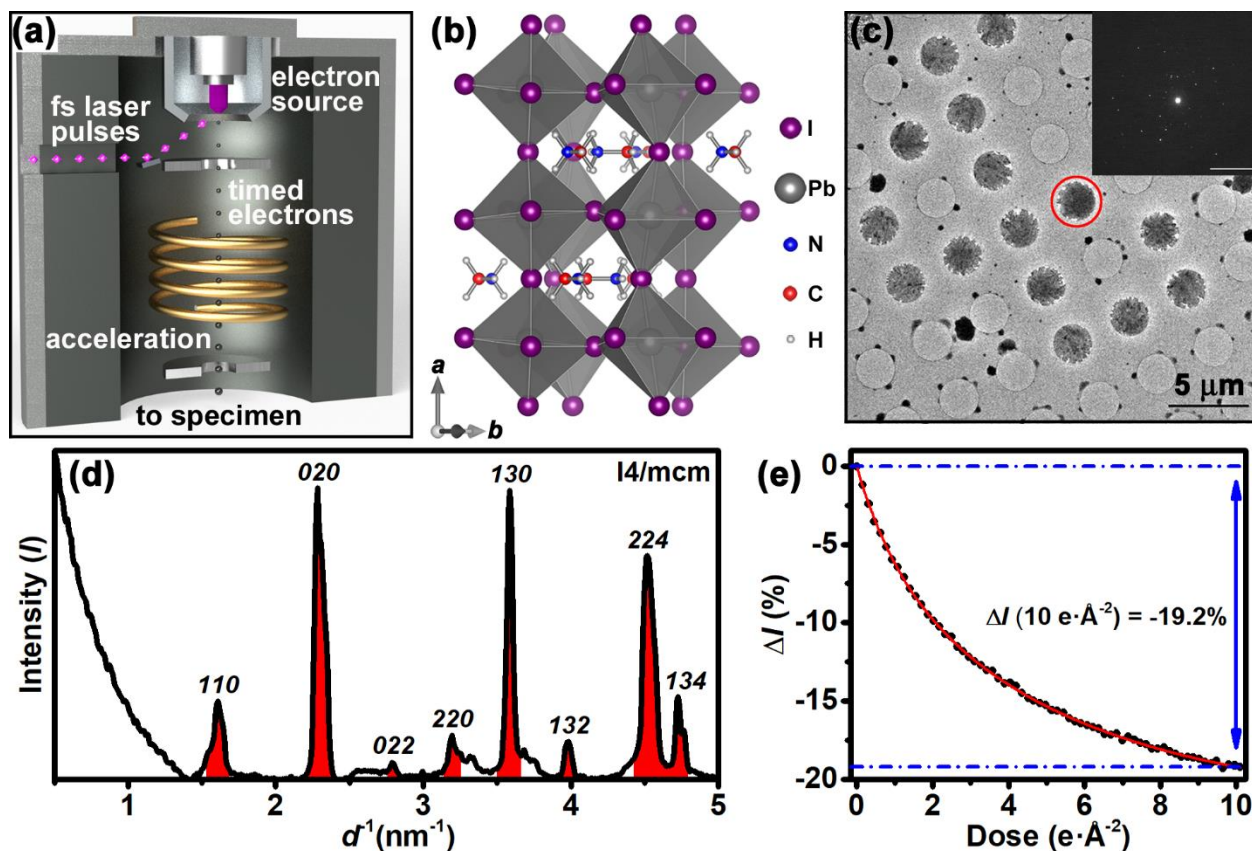
Figure 1. Laser-driven pulsed-beam TEM. (a) Simplified schematic of the electron-source region. (b) Structure of MAPbI$_3$.[24] (c) Bright-field image of the TEM specimens. The diffraction pattern (inset; scale bar = 5 nm^{-1}) was obtained from the red-circled region. (d) Intensity plot from azimuthally averaging the pattern in (c). Red peaks are those used for monitoring beam-induced intensity changes. The space group used for indexing was *I4/mcm*.[25] (e) Bragg-intensity fading curve for a pulsed beam (dose rate = 0.001 e·Å^{-2}·s^{-1}; beam size = 245 ± 3 μm^2; 50.4 ± 1.0 e/p; f = 500 kHz). Red curve is to determine ΔI at 10 e·Å^{-2}.

Specimens were synthesized by spin coating a 0.3-M solution of MAPbI$_3$ with 10% molar excess MAI in a 4:1 volume ratio of DMF:DMSO onto holey amorphous-carbon grids (Fig. 1b,c). First, the grid was reversibly adhered to a Si support using a drop of toluene

followed by heating at 100 °C (1 min.). Next, 0.2 mL of MAPbI$_3$ solution was dropped onto the supported grid while spinning at 3000 rpm for 2 min. Finally, the grid was annealed at 100 °C (1 hr.). This produced freestanding, polycrystalline MAPbI$_3$ islands spanning the 2.5-µm holes of the grids (Fig. 1c,d). Accordingly, each island was 4.8 ± 0.2 µm^2 in area. Damage was quantified using a fading-curve method, where a reduction in Bragg-beam intensities (ΔI; indicative of destruction of MAPbI$_3$ crystalline order) was tracked as a function of dose (Fig. 1e).[26] Peaks arising from planes with $d < 6.3$ Å were summed and monitored as a function of accumulated dose. Note $\Delta I = (I - I_o)/I_o$, which is the normalized change in intensity relative to that at nominally zero dose (I_o). A dose of 10 e·Å^{-2} was used as the reference point throughout.

Comparison of damage caused to MAPbI$_3$ by a pulsed beam to that of a conventional thermionic beam is shown in Figure 2. For a common dose rate (0.001 e·Å^{-2}·s^{-1} for an illuminated area of 245 ± 3 µm^2), there is a clear reduction in the extent to which the intensities fade for the pulsed beam under the conditions used for this experiment (50.4 ± 1.0 e/p and $f^1 = 2$ µs). At 10 e·Å^{-2}, the intensity change for the pulsed beam is -19.2%, while that of the thermionic beam is -23.2%. This shows that providing temporally-regular pauses in electron-beam irradiation, thus providing regular periods of specimen relaxation and a reduction in exacerbating effects (*e.g.*, multi-electron impact within a specific damage radius), leads to enhanced preservation of MAPbI$_3$ structural order compared to conventional low-dose methods. Note that for pulsed-beam TEM experiments performed on C$_{36}$H$_{74}$ and bacteriorhodopsin, the extent to which damage was reduced was greater than seen here, though evidence indicates the degree of reduction also depends on f^1.[17,19] This suggests the extent to which damage is reduced is largely material dependent while the overall effect of pulsed beams is a general phenomenon.
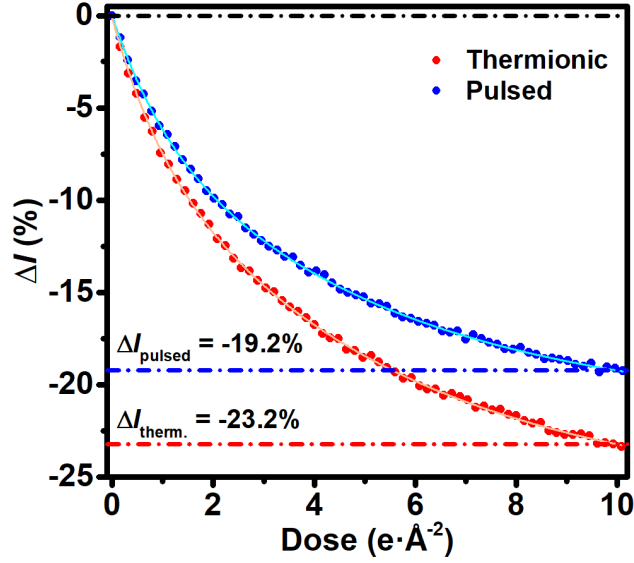
Figure 2. Fading curves for MAPbI$_3$ for pulsed (blue; also shown in Fig. 1e) and thermionic (red) beams delivered at the same dose rate (0.001 e·Å^{-2}·s^{-1}). Fits to the data are for determining ΔI at 10 e·Å^{-2}. Illuminated area was 245 ± 3 μm^2 for both. The pulsed beam consisted of 50.4 ± 1.0 e/p and $f^{-1} = 2$ μs.

Drawing conclusions from direct comparisons requires control of myriad variables that influence, interfere with, and overwhelm intrinsic beam-damage behavior (*e.g.*, specimen thickness, specimen bending, lab temperature stability, specimen and beam drift, *etc.*). Controls performed in our lab when conducting pulsed-beam damage experiments are described elsewhere.[17] As an example here, experiments were rejected and repeated when the beam current, as well as the beam size, differed by more than 1% before and after acquisition of a data series. Experiments were conducted after observable directional specimen drift ceased. Further, experiments were rejected if the specimen was found to have directionally drifted more than 1% of the substrate hole diameter (*i.e.*, 25 nm) between the start and finish of data acquisition. Data presented here consists of multiple experimental trials conducted over several days.

To better understand the origins of damage reduction using a pulsed beam, effects of varying e/p and f^{-1} were explored (Fig. 3). Depending upon the mechanisms at work, one might expect an increase in damage with increased e/p and also with decreased f^{-1}.[17-19] However, regimes exist wherein benefits gained by having additional specimen relaxation and recovery time between pulses are lost when simultaneously introducing more electrons per pulse.[17] This is indeed the case for MAPbI$_3$. For both 0.001 e·Å^{-2}·s^{-1} and 0.01 e·Å^{-2}·s^{-1} (Fig. 3a and 3b, respectively), damage increases with increased e/p despite an increased f^{-1} from 2 μs to 4 μs for the larger electron pulses. This suggests that specimen relaxation and recovery processes at work during the few microseconds between pulses are overwhelmed by exacerbating effects of simultaneous or near-simultaneous multi-electron impact within a given damage radius. That is, additional energy deposited into the already-excited specimen region causes structural damage that otherwise may have recovered during a single electron event isolated in space and time.
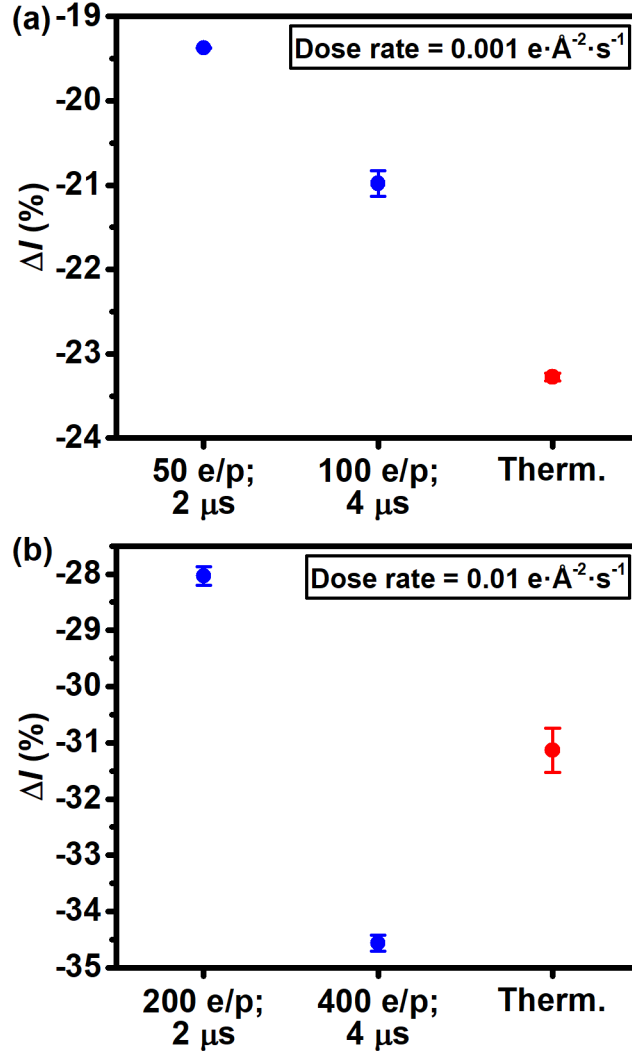
Figure 3. Effect of e/p and f^{-1} on damage to MAPbI$_3$ for a total dose of 10 e·Å^{-2}. (a) Bragg-intensity reduction for pulsed (blue) and thermionic (therm., red) methods administered at a dose rate of 0.001 e·Å^{-2}·s^{-1}. Time between electron pulses (f^{-1}) is shown below the number of electrons per pulse (e/p). Error bars for 50 e/p, 100 e/p, and thermionic are one standard deviation over 2, 4, and 2 separate experiments, respectively. (b) Bragg-intensity reduction for pulsed (blue) and thermionic (therm., red) methods administered at a dose rate of 0.01 e·Å^{-2}·s^{-1}. Error bars for 200 e/p, 400 e/p, and thermionic are one standard deviation over 2, 2, and 3 separate experiments, respectively.

As with $C_{36}H_{74}$, a threshold exists for MAPbI$_3$, where a pulsed beam causes more damage than a thermionic beam (Fig. 3b).[17] The instantaneous dose rate for a single pulse of 400 electrons confined to 300 fs (more likely a few picoseconds due to Coulombic expansion)[27] equates to 5 x 10^4 e·Å^{-2}·s^{-1}, assuming uniform illumination across the 245-µm^2 beam area. It is therefore perhaps surprising that such a beam does not produce substantially more damage than observed, though the number of electrons per Å^2 per pulse is only 2 x 10^{-8}. Such a low area number density suggests that, if cooperative effects are a significant source of damage, the pulse-to-pulse illumination may not be uniform. Though unlikely here, such a situation could arise from spatial pulse-to-pulse laser jitter for specimens that are on the order of the size of the beam. Each pulse may then arrive at different specimen regions despite the time-averaged beam being uniformly spread. Though the time-averaged reduction in damage for pulsed beams is clear, pulse-to-pulse behaviors and the resulting specimen effects are largely unknown.

The results in Figures 2 and 3 demonstrate that clear, repeatable differences exist between pulsed and random beams in the TEM. Evidence suggests that this is driven by temporal processes that are active on the pulse-to-pulse timescales.[15-19] Such processes include thermal effects which, while not yet well understood for electron-beam excitation and damage in MAPbI$_3$, are important in similar low-thermal-conductivity materials.[23,26,28] The effect of thermal processes in damage reduction can be appreciated by noting timescales of thermal diffusion and relaxation in MAPbI$_3$ relative to f^{-1}. Using known constants,[29-32] it is estimated that thermal energy deposited into a 2.5-µm diameter MAPbI$_3$ crystal would largely dissipate into the carbon substrate within several microseconds. Note, however, that temperature from the perspective of the entire specimen is likely too coarse a view when considering pulsed-beam damage mechanisms and temporal aspects of molecular-scale excitations. Nevertheless, this

estimate indicates thermal-dissipation times are comparable to f^{-1}, suggesting complete relaxation prior to a subsequent event is a plausible source of reduced damage.

Timescales of electron-phonon coupling and lattice thermalization are also relevant. Electron-phonon coupling in MAPbI$_3$ films occurs on the order of hundreds of femtoseconds, while lattice thermalization takes a few picoseconds.[33] Owing to the electron-pulse duration, most or all will arrive within this time frame. Further, increasing e/p generally causes an increase in pulse duration,[27] thus creating an environment where the likelihood of exacerbating effects contributing to damage is increased. Systematic pulse duration experiments may shed light on these effects. Similar arguments can be made regarding specimen charging, charge dissipation, and electron-pulse durations and timing.

In conclusion, for common total doses and dose rates, we have discovered a regime where using a pulsed-beam TEM leads to reduced damage to MAPbI$_3$. The degree of reduction is enhanced by using pulses with fewer electrons, while the duration between pulses appears to have a smaller but still non-trivial effect. We also discover a threshold effect, in which pulsed beams cause more damage than an otherwise identical conventional beam. These results have fundamental and practical implications, in that fs-laser-driven pulsed TEM offers a combination of stability and tunability that affords studying specific damage mechanisms in MAPbI$_3$ as well as providing structural, chemical, electronic, and dynamic information from less-damaged specimens.

*Author to whom correspondence should be addressed.

Email: flan0076@umn.edu

Office: +1 612-625-3867

Author Contributions: EJV contributions were formal analysis, investigation, methodology, software, validation, visualization, writing – original draft, writing – review and editing. CPC contributions were investigation, methodology, specimen preparation, writing – original draft, and writing – review and editing. RJH contributions were conceptualization, funding acquisition, project administration, supervision, and writing – review and editing. DJF contributions were conceptualization, formal analysis, funding acquisition, methodology, project administration, resources, supervision, visualization, writing – original draft, writing – review and editing.

Competing Interests: Authors declare no competing interests.

References:

(1)   Egger, D. A.; Bera, A.; Cahen, D.; Hodes, G.; Kirchartz, T.; Kronik, L.; Lovrincic, R.; Rappe, A. M.; Reichman, D. R.; Yaffe, O. What Remains Unexplained about the Properties of Halide Perovskites? *Adv. Mater.* **2018**, *30*, 1800691.

(2)   *Best Research-Cell Efficiency Chart*, National Renewable Energy Laboratory, Accessed July 2020, https://www.nrel.gov/pv/cell-efficiency.html

(3)   Doherty, T. A. S.; Winchester, A. J.; Macpherson, S.; Johnstone, D. N.; Pareek, V.; Tennyson, E. M.; Kosar, S.; Kosasih, F. U.; Anaya, M.; Abdi-Jalebi, M.; Andaji-Garmaroudi, Z.; Wong, E. L.; Madéo, J.; Chiang, Y.-H.; Park, J.-S.; Jung, Y.-K.; Petoukhoff, C. E.; Divitini, G.; Man, M. K. L.; Ducati, C.; Walsh, A.; Midgley, P. A.; Dani, K. M.; Stranks, S. D. Performance-Limiting Nanoscale Trap Clusters at Grain Junctions in Halide Perovskites. *Nature* **2020**, *580*, 360-366.

(4)   Ran, J.; Dyck, O. O.; Wang, X.; Yang, B.; Geohegan, D. B.; Xiao, K. Electron-Beam-Related Studies of Halide Perovskites: Challenges and Opportunities. *Adv. Energy Mater.* **2020**, *10*, 1903191.

(5)   Divitini, G.; Cacovich, S.; Matteocci, F.; Cinà, L.; Di Carlo, A.; Ducati, C. *In Situ* Observation of Heat-Induced Degradation of Perovskite Solar Cells. *Nat. Energy* **2016**, *1*, 15012.

(6)   Rothmann, M. U.; Li, W.; Zhu, Y.; Liu, A.; Ku, Z.; Bach, U.; Etheridge, J.; Cheng, Y. B. Structural and Chemical Changes to $CH_3NH_3PbI_3$ Induced by Electron and Gallium Ion Beams. *Adv. Mater.* **2018**, *30*, 1800629.

(7)   He, J.; Liu, Z.; Cao, Z.; Zhang, H.; Meng, Y.; Chen, B.; Zhong, D. Visualizing the Redox Reaction Dynamics of Perovskite Nanocrystals in Real and Reciprocal Space. *J. Phys. Chem. Lett.* **2020**, *11*, 2550-2558.

(8)   Ball, J. M.; Petrozza, A. Defects in Perovskite-Halides and Their Effects in Solar Cells. *Nat. Energy* **2016**, *1*, 16149.

(9)   Rothmann, M. U.; Li, W.; Zhu, Y.; Bach, U.; Spiccia, L.; Etheridge, J.; Cheng, Y.-B. Direct Observation of Intrinsic Twin Domains in Tetragonal $CH_3NH_3PbI_3$. *Nat. Commun.* **2017**, *8*, 14547.

(10)   Chen, S.; Zhang, X.; Zhao, J.; Zhang, Y.; Kong, G.; Li, Q.; Li, N.; Yu, Y.; Xu, N.; Zhang, J.; Liu, K.; Zhao, Q.; Cao, J.; Feng, J.; Li, X.; Qi, J.; Yu, D.; Li, J.; Gao, P. Atomic Scale Insights into Structure Instability and Decomposition Pathway of Methylammonium Lead Iodide Perovskite. *Nat. Commun.* **2018**, *9*, 4807.

(11)   Alberti, A.; Bongiorno, C.; Smecca, E.; Deretzis, I.; Magna, A. L.; Spinella, C. Pb Clustering and PbI_2 Nanofragmentation during Methylammonium Lead Iodide Perovskite Degradation. *Nat. Commun.* **2019**, *10*, 2196.

(12) Yu, Y.; Zhang, D.; Kisielowski, C.; Dou, L.; Kornienko, N.; Bekenstein, Y.; Wong, A. B.; Alivisatos, A. P.; Yang, P. Atomic Resolution Imaging of Halide Perovskites. *Nano Lett.* **2016**, *16*, 7530−7535.

(13) Li, Y.; Zhou, W.; Li, Y.; Huang, W.; Zhang, Z.; Chen, G.; Wang, H.; Wu, G.-H.; Rolston, N.; Vila, R.; Chiu, W.; Cui, Y. Unravelling Degradation Mechanisms and Atomic Structure of Organic-Inorganic Halide Perovskites by Cryo-EM. *Joule* **2019**, *3*, 2854-2866.

(14) Chen, X.; Wang, Z. Investigating Chemical and Structural Instabilities of Lead Halide Perovskite Induced by Electron Beam Irradiation. *Micron* **2019**, *116*, 73-79.

(15) Flannigan, D. J.; Lobastov, V. A.; Zewail, A. H. Controlled Nanoscale Mechanical Phenomena Discovered with Ultrafast Electron Microscopy. *Angew. Chem. Int. Ed.* **2007**, *46*, 9206-9210.

(16) Kwon, O. H.; Ortalan, V.; Zewail, A. H. Macromolecular Structural Dynamics Visualized by Pulsed Dose Control in 4D Electron Microscopy. *Proc. Natl. Acad. Sci. U.S.A.* **2011**, *108*, 6026-6031.

(17) VandenBussche, E. J.; Flannigan, D. J. Reducing Radiation Damage in Soft Matter with Femtosecond-Timed Single-Electron Packets. *Nano Lett.* **2019**, *19*, 6687-6694.

(18) Kisielowski, C.; Specht, P.; Freitag, B.; Kieft, E. R.; Verhoeven, W.; van Rens, J. F. M.; Mutsaers, P.; Luiten, J.; Rozeveld, S.; Kang, J.; McKenna, A. J.; Nickias, P.; Yancey, D. F. Discovering Hidden Material Properties of $MgCl_2$ at Atomic Resolution with Structured Temporal Electron Illumination of Picosecond Time Resolution. *Adv. Funct. Mater.* **2019**, *29*, 1807818.

(19) Choe, H.; Ponomarev, I.; Montgomery, E.; Lau, J. W.; Zhu, Y.; Zhao, Y.; Liu, A.; Kanareykin, A.; Jing, C. Mitigation of Radiation Damage in Macromolecules via Tunable Ultrafast Stroboscopic TEM. *bioRxiv* **2020**, 2020.2005.2015.099036.

(20) Lang, F.; Nickel, N. H.; Bundesmann, J.; Seidel, S.; Denker, A.; Albrecht, S.; Brus, V. V.; Rappich, J.; Rech, B.; Landi, G.; Neitzert, H. C. Radiation Hardness and Self-Healing of Perovskite Solar Cells. *Adv. Mater.* **2016**, *28*, 8726-8731.

(21) Nie, W.; Blancon, J.-C.; Neukirch, A. J.; Appavoo, K.; Tsai, H.; Chhowalla, M.; Alam, M. A.; Sfeir, M. Y.; Katan, C.; Even, J.; Tretiak, S.; Crochet, J. J.; Gupta, G.; Mohite, A. D. Light-Activated Photocurrent Degradation and Self-Healing in Perovskite Solar Cells. *Nat. Commun.* **2016**, *7*, 11574.

(22) Ceratti, D. R.; Rakita, Y.; Cremonesi, L.; Tenne, R.; Kalchenko, V.; Elbaum, M.; Oron, D.; Potenza, M. A. C.; Hodes, G.; Cahen, D. Self-Healing inside $APbBr_3$ Halide Perovskite Crystals. *Adv. Mater.* **2018**, *30*, 1706273.

(23) Egerton, R. F. Radiation Damage to Organic and Inorganic Specimens in the TEM. *Micron* **2019**, *119*, 72-87.

(24)   Momma, K.; Izumi, F. VESTA 3 for Three-Dimensional Visualization of Crystal, Volumetric and Morphology Data. *J. Appl. Crystallogr.* **2011**, *44*, 1272–1276.

(25)   Yamada, Y.; Yamada, T.; Phuong, L. Q.; Maruyama, N.; Nishimura, H.; Wakamiya, A.; Murata, Y.; Kanemitsu, Y. Dynamic Optical Properties of $CH_3NH_3PbI_3$ Single Crystals As Revealed by One- and Two-Photon Excited Photoluminescence Measurements. *J. Am. Chem. Soc.* **2015**, *137*, 10456-10459.

(26)   Grubb, D. T. Radiation Damage and Electron Microscopy of Organic Polymers. *J. Mater. Sci.* **1974**, *9*, 1715-1736.

(27)   Plemmons, D. A.; Flannigan, D. J. Ultrafast Electron Microscopy: Instrument Response from the Single-Electron to High Bunch-Charge Regimes. *Chem. Phys. Lett.* **2017**, *683*, 186-192.

(28)   Fryer, J. R. Radiation Damage in Organic Crystalline Films. *Ultramicroscopy* **1984**, *14*, 227-236.

(29)   Pisoni, A.; Jaćimović, J.; Barišić, O. S.; Spina, M.; Gaál, R.; Forró, L.; Horváth, E. Ultra-Low Thermal Conductivity in Organic–Inorganic Hybrid Perovskite $CH_3NH_3PbI_3$. *J. Phys. Chem. Lett.* **2014**, *5*, 2488-2492.

(30)   Qian, X.; Gu, X.; Yang, R. Lattice Thermal Conductivity of Organic-Inorganic Hybrid Perovskite $CH_3NH_3PbI_3$. *Appl. Phys. Lett.* **2016**, *108*, 063902.

(31)   Onoda-Yamamuro, N.; Matsuo, T.; Suga, H. Calorimetric and IR Spectroscopic Studies of Phase Transitions in Methylammonium Trihalogenoplumbates. *J. Phys. Chem. Solids* **1990**, *51*, 1383-1395.

(32)   Baikie, T.; Barrow, N. S.; Fang, Y.; Keenan, P. J.; Slater, P. R.; Piltz, R. O.; Gutmann, M.; Mhaisalkar, S. G.; White, T. J. A Combined Single Crystal Neutron/X-ray Diffraction and Solid-State Nuclear Magnetic Resonance Study of the Hybrid Perovskites $CH_3NH_3PbX_3$ (X = I, Br and Cl). *J. Mater. Chem. A* **2015**, *3*, 9298-9307.

(33)   Ghosh, T.; Aharon, S.; Etgar, L.; Ruhman, S. Free Carrier Emergence and Onset of Electron–Phonon Coupling in Methylammonium Lead Halide Perovskite Films. *J. Am. Chem. Soc.* **2017**, *139*, 18262-18270.